A single-molecule enzymatic assay in a directly accessible femtoliter droplet array†

Shouichi Sakakihara,[a] Suguru Araki,[ab] Ryota Iino*[ab] and Hiroyuki Noji*[abc]

Received 1st June 2010, Accepted 14th September 2010
DOI: 10.1039/c0lc00062k

The enzyme assay in a femtoliter chamber array is a simple and efficient method for concentrating the reaction product; it greatly improves the detection sensitivity down to the single-molecule level. However, in previous methods, controlling the initiation and termination of the reaction in each chamber is difficult once enclosed. Furthermore, the recovery of the enzyme and product is also difficult. To overcome these drawbacks, we developed a femtoliter droplet array in which the individual droplets are fixed on the substrate and are directly accessible from outside. A hydrophilic-in-hydrophobic micropatterned surface was used for the preparation of the droplets. When the aqueous solution on the surface is exchanged with oil, the hydrophilic surface retains the aqueous solution, and more than 10^6 dome-shaped droplets that are usable for further assay can be prepared simultaneously. The curvature radius of the droplet obeys the Young–Laplace equation, and the volume can be precisely controlled by the micropipette, which applies pressure into the droplet. Changing the pressure makes the addition, collection, and exchange of the aqueous content for individual droplets possible. Using these advantages, we successfully measured the kinetic parameters of the single-molecule enzyme β-galactosidase and rotary motor protein F_1-ATPase enclosed in a droplet.

Introduction

Reducing the assay volume by miniaturizing experimental systems is a major topic for lab-on-a-chip (LOC) and micro-total-analysis-system (μTAS) technologies being applied in biology.[1–4] Doing so makes it possible to achieve high-throughput measurements while saving precious samples and expensive reagents. Reaction chambers with volume scales of picoliters have been fabricated by combining polydimethylsiloxane (PDMS) microchannels and valves.[5,6] In these systems, the solutions in the chambers separated by a valve can be mixed and separated again by opening and closing the valve; control of the reaction initiation and termination is possible. This has been successfully applied to counting low copy numbers of protein in single cells.[7–9] In addition to the chamber array consisting of the PDMS channel and valve, water-in-oil emulsion microdroplets have also been often used as microreactors.[10–14] Many droplets can be rapidly generated in the microchannel at rates of up to 30 kHz; this allows for the preparation of high-density microdroplet arrays.[15] Since droplets in an array tend to spontaneously fuse with each other, amphipathic detergents are usually added for stabilization. Nontoxic and biocompatible detergents have recently been developed, because many detergents exhibit unwanted effects on biological samples such as denaturation of the proteins and cell toxicity.[15,16] Controlled coalescence of droplets can be used to merge the contents and initiate the reaction.[17–20]

Further reduction of the assay volume to the femtoliter level provides a significant advantage for highly sensitive detection of enzyme reactions down to the single-molecule level; a very small amount of reaction products confined to femtoliter volumes results in a very high concentration and makes it possible to apply conventional detection methods such as fluorescence. However, decreasing the reaction volume to the femtoliter level in channel-valve PDMS chambers and droplet arrays is not easy. The channel-valve chambers need many connections to the outside for controlling the air pressure or the flow of liquids, making the device relatively large and complicated. Generating a stable array of droplets with the size of several micrometers is not easy even in the presence of detergents.

In a previous study, we developed a simple method for easily preparing a femtoliter chamber array for the single-molecule assay of enzymatic reactions.[21–24] In our previous method, the chamber was prepared by sandwiching the sample solution between a PDMS or polyacrylamide (PAA) gel with many microcavities on the surface and a coverglass. Following our study, other types of femtoliter chambers have been prepared by bundling optical fibers with microcavities on the tip and with silicon sheets,[25,26] or combining PDMS microwells with valve in the microchannel.[27] Using fluorogenic substrates, the single-molecule enzymatic activity of β-galactosidase and horseradish peroxidase enclosed in the chamber can easily be measured under a conventional epi-fluorescence microscope.[21,25,27] By combining the PDMS chamber with a single-molecule manipulation technique (magnetic tweezers),[28] the chemomechanical coupling efficiency of a rotary motor protein F_1-ATPase (F_1) was

[a]*Institute of Scientific and Industrial Research, Osaka University, Mihogaoka, 8-1, Ibaraki, Osaka, 567-0047, Japan. E-mail: iino@sanken.osaka-u.ac.jp; Fax: +81-6875-5724; Tel: +81-6879-8481; hnoji@sanken.osaka-u.ac.jp; +81-6875-5724; +81-6879-8481*
[b]*CREST, Japan Science and Technology Agency, Sanbancho 5, Chiyoda-ku, Tokyo 102-0075, Japan*
[c]*Department of Applied Chemistry, Graduate School of Engineering, The University of Tokyo, Hongo 7-3-1, Bunkyo-ku, Tokyo 113-8656, Japan*
† Published as part of a LOC themed issue dedicated to Japanese Research: Guest Editor Professor Yoshinobu Baba.

estimated.[29–31] In addition, PAA chambers that can transfer small molecules into the chamber through the gel matrix have been applied to the single-molecule analysis of DNA. Cleavage of a single DNA molecule with a restriction enzyme triggered by magnesium ion influx into the PAA chamber and direct size estimation of free-standing DNA fragments elongated by electrostretching in the PAA chamber have been carried out.[22] The PAA chamber has also been applied to amplification of a single DNA molecule by loop-mediated isothermal amplification.[32]

As mentioned above, femtoliter chambers with solid microcavities are simple and versatile; they can be easily combined with other single-molecule techniques based on optical microscopy. However, they have two drawbacks: both access to individual chambers and the manipulation of the content are difficult. In this manuscript, we report the development of a detergent-free, femtoliter droplet array fixed on a hydrophilic-in-hydrophobic patterned surface.[33,34] In our new method, more than 10^6 dome-shaped droplets that are usable for further assay can be prepared simultaneously. The most prominent feature is that we can access and manipulate the individual droplets from outside using a micropipette. The volume of individual droplets can be precisely controlled; furthermore, the addition, collection, and exchange of the aqueous content in an individual droplet are possible. Because of these advantages, we could successfully measure the kinetic parameters of single-molecule enzymes such as β-galactosidase and F_1 enclosed in the droplet.

Experimental

Preparation of hydrophilic-in-hydrophobic micropatterned surface

A hydrophobic polymer of carbon-fluorine (CYTOP, Asahi-glass) diluted to 0.84 wt% with a solvent (CT-solv. 180, Asahi-glass) was spin-coated on a cleaned coverglass (30 mm in diameter, Matsunami) at 4000 rpm; it was then baked for 1 h at 180 °C. Photolithography was carried out with a high-viscosity photoresist (AZP4903, AZ Electronic Materials) because the CYTOP-coated surface had very low friction and could not be fully covered with a low-viscosity photoresist. The resist-patterned substrate surface was dry-etched with O_2 plasma by a reactive ion etching system (RIE-10NR, Samco) to expose the hydrophilic SiO_2 glass surface. The thickness of the CYTOP layer was 17 nm as measured by an atomic force microscope (VN-800, KEYENCE).

General methods of droplet array formation

The hydrophilic-in-hydrophobic micropatterned coverglass was attached to the bottom of a perforated Petri dish (35 mm in diameter) and covered with aqueous solution. Oil (Fluorinert FC40, Sigma), which has a higher density than water, was then flowed into the aqueous solution near the substrate surface. The hydrophilic SiO_2 glass surface retained the aqueous solution, while the hydrophobic surface was covered with oil. As a result, many droplets were formed simultaneously. To form individual droplets one-by-one, the patterned coverglass was covered with the oil first, and the aqueous solution in the micropipette was ejected by contacting the hydrophilic surface.

Measurement of the curvature radius of the droplet

Droplets were formed by attaching a micropipette (Femtochip, Eppendorf) onto the hydrophilic surface of the patterned substrate covered with Fluorinert FC40 at various pressures using a micromanipulator (MNM-21, Narishige) and pressure controller (Femtojet, Eppendorf). The micropipette was filled with 200 or 500 μM fluorescein (Invitrogen) in buffer A (100 mM potassium phosphate, 0.02% 2-mercaptoethanol, 2 mM $MgCl_2$, pH 7.5). The fluorescence images of the droplets were obtained by an inverted microscope (Ti-E, Nikon) equipped with a confocal unit (CSU-X1, Yokogawa). The 3D images of the droplet were constructed by software (NIKON) using slice images taken along the *Z*-axis with intervals of 0.26 or 0.13 μm. The curvature radius was determined from the image by ImageJ software assuming that the droplet fixed on hydrophilic pattern is part of a sphere.

Single-molecule enzymatic assay of β-galactosidase activity

β-Galactosidase (β-gal) and fluorescein-di-β-garactopyranoside (FDG) were purchased from Roche and Invitrogen, respectively. Other chemicals were purchased from Wako. The injection of β-gal (0.16 or 0.4 nM) and FDG (1 mM) in buffer A into the droplet were carried out using a micropipette (Femtochip, Eppendorf) equipped with a pressure controller (Femtojet, Eppendorf). The phase-contrast and epi-fluorescence images of the droplets were obtained simultaneously under an inverted microscope (IX-71, Olympus) and were recorded by a digital video recorder (DSR10, Sony). The recorded images were captured and sent to a PC by a frame grabber board (Himawari PCI, Library) as an 8-bit AVI file and analyzed by ImageJ software. Conversion from fluorescence intensity to fluorescein concentration was carried out by measuring the fluorescence intensity of droplets which contained known concentrations of fluorescein solution.

Single-molecule rotation assay of F_1-ATPase in droplet

The $\alpha(His_6$ at N-terminus/C193S$)_3\beta(His_3$-Lys_7 at N-terminus$)_3\gamma$(S108C/I211C) subcomplex of the F_1-ATPase (F_1) was used for the single-molecule rotation assay. F_1 was prepared as previously described.[35] To attach a probe of rotation to the rotor γ subunit of F_1, biotin-PEO4-maleimide (Dojin) was reacted with thiol groups of two cysteine resides of the γ. The probe visualizing the rotation of F_1, the streptavidin-coated polystylene bead was prepared in the lab as follows. The 220-nm polystyrene beads (Polybead Amino 0.20 micron Microspheres, Polysciences) were reacted with Biotin-PEO4-NHS (Thermo scientific) and bound with streptavidin (Type II, Wako).

The single-molecule rotation assay of F_1 was carried out under an inverted microscope (IX71, Olympus). First, the patterned substrate attached to the perforated Petri dish (35 mm in diameter) was covered with 1 mL of a buffer (10 mM potassium phosphate, pH 8.0) containing 800 pM F_1; this was incubated for 10–15 min at room temperature to bind the stator $\alpha_3\beta_3$ ring of F_1 to the hydrophilic SiO_2 surface. The stator $\alpha_3\beta_3$ was immobilized on the glass by the electrostatic interaction between the positively charged poly-lysine residues introduced into the amino-terminus of β subunits and the negatively charged glass surface. To remove

unbound F_1, 700 μL of buffer was removed, and 1 mL of fresh buffer without F_1 was added. The removal and addition of the buffer were repeated five times, and 300 μL of the buffer was left to avoid evaporation. The buffer was replaced with 1 mL Fluorinert FC40 to form droplet array containing F_1. Excess buffer was added on the top of Fluorinert FC40 to suppress evaporation. Next, to block the nonspecific binding of the streptavidin-coated beads to the hydrophilic surface, 5 mg/mL bovine serum albmin and 500 nM ATP in buffer B (10 mM potassium phosphate, 1 mM phosphoenolpyruvate, 0.1 mg/mL pyruvate kinase, 2 mM $MgCl_2$, pH 8.0) were injected by attaching the micropipette (Femtochip, Eppendorf) for 5 s at 40–50 hPa (1 hPa = 100 Pa). The bead suspension containing 10 μM ATP in buffer C (10 mM potassium phosphate, 2 mM $MgCl_2$, pH 8.0) was then injected for 5 s at 50–60 hPa, by attaching a micropipette (inside aperture 5–10 μm) prepared from a capillary (75 μL, Drummond Scientific) using a puller (Model PC10, Narishige) and microforge (MF900, Narishige). After finding the rotating particles, the ATP concentration ([ATP]) was changed by attaching other micropipettes (Femtochip, Eppendorf, inside aperture 0.5 μm) filled with different [ATP] in buffer B for 30 s at 40–50 hPa. Phase-contrast images of the rotating beads were recorded to a digital video recorder (DSR10, Sony), and the rotation rate was analyzed by custom software (Digimo).

Results and discussion

Formation and volume control of the droplet

An example of the hydrophilic-in-hydrophobic micropatterned surface is shown in Fig. 1A. In our method, the droplet array is formed very readily (Fig. 1B). First, the micropatterned surface is covered with a aqueous solution. The oil (Fluorinert FC40), which has a higher density than water, is then loaded into the aqueous solution. The hydrophilic SiO_2 glass surface retains the aqueous solution, while hydrophobic surface does not and replaces it with oil; more than 10^5 droplets are formed simultaneously on this pattern (Fig. 1C). The size and density of the droplets can be easily modulated by changing the pattern, and the number of droplets formed simultaneously can be easily increased by preparing the patterned surface with a larger area. So far, we have achieved the formation of 1×10^6 droplets in an area of 100 mm^2 using the 4.8 μm (in diameter) hydrophilic patterns spaced by 10 μm (center-to-center distance between patterns) in hexagonal close packing.

The droplets do not have solid walls but are isolated from each other by oil; they are accessible from outside. Access to individual droplets can be achieved by a commercially available micropipette (Femtochip) and a pressure controller connected to the micropipette, which is generally used for injection into mammalian cell lines. When relatively high pressure is applied inside the micropipette and the tip is attached to the preformed droplet, the solution in the micropipette can be injected. The solution is not ejected from the micropipette unless the tip touches the droplet due to the large interfacial tension between water and oil. Fig. 2A shows a heart-mark frame formed by the injection of water at a pressure of 80 hPa. In contrast, when we set the pressure inside the micropipette to 0 hPa and contact the tip to the droplet, the solution in the droplet is sucked into the

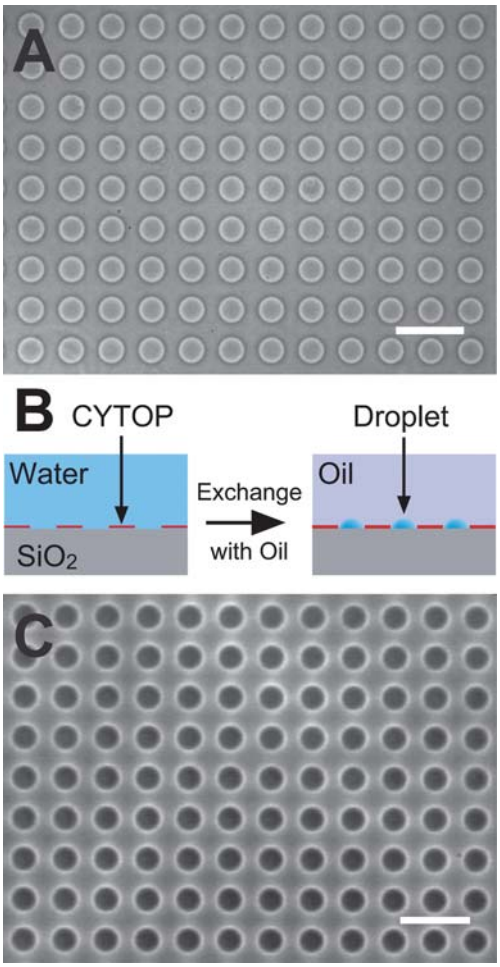

Fig. 1 Formation of femtoliter droplet array. (A) An example of the hydrophilic-in-hydrophobic micropatterned surface. Hydrophilic SiO_2 circular patterns (20 μm in diameter) in the hydrophobic polymer (CYTOP) layer. (B) Schematic drawing of droplet array preparation procedure. Water on the micropatterned surface is exchanged with oil. (C) Droplet array formed on surface. Scale bars: 50 μm.

micropipette by capillary force (Fig. 2A right, inside the heart-mark). As shown here, the volume of the droplet can be regulated by applying pressure inside the micropipette. The flow through the aperture of the micropipette stops spontaneously when the pressure inside the micropipette is balanced with interfacial tension of the droplet. The critical contact angle of $\pi/2$ seemed to be the upper limit for the formation of a stable droplet as reported previously.[33,34] When the pressure higher than a critical value (see below) was applied, the flow from the micropipette no longer stopped and the droplet continued to expand.

Fig. 2B shows fluorescence images of three droplets containing fluorescein; these images were obtained with a confocal microscope. These droplets were formed on hydrophilic circular patterns with diameters of 20 μm at pressures of 80, 60, and 40 hPa. Using the fluorescence images, we measured the heights of droplets formed on the hydrophilic circular patterns with different diameters and calculated the curvature radii assuming that they formed partial spheres (Fig. 2C). The pattern is fully covered with buffer solution after the droplet formation and the diameter at the bottom of droplet is same as that of circular

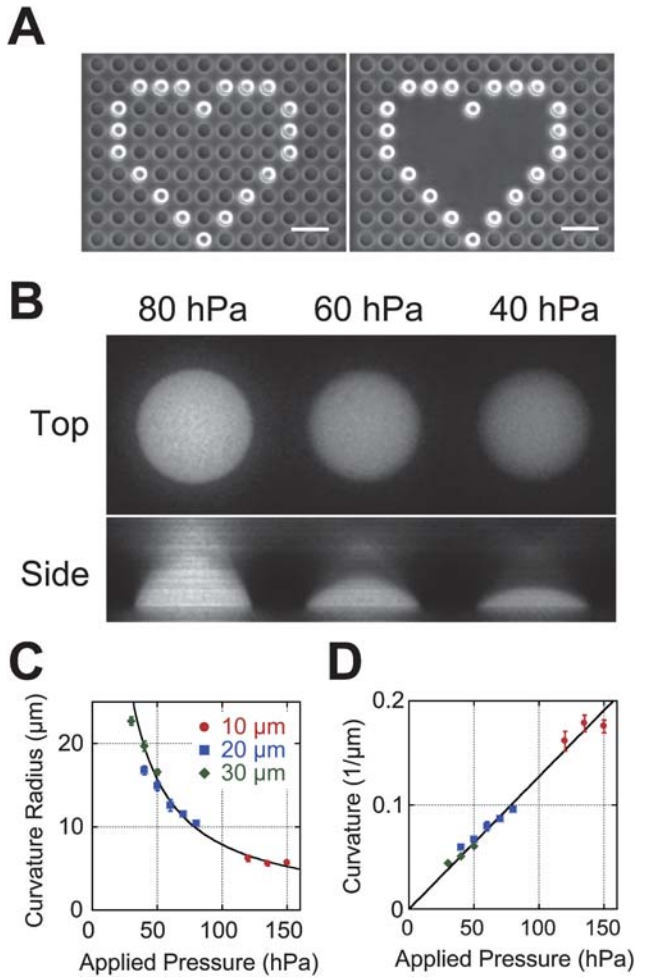

Fig. 2 Volume control of the droplet by micropipette. (A) *Left*: A heart-mark frame formed by injection of water with a micropipette at 80 hPa on 20 μm circular patterns. In the phase-contrast image, the high side-walls of droplets look white. *Right*: Droplets inside the heart-mark were sucked out at 0 hPa. Scale bars: 50 μm. (B) Top and side view images of the droplets formed on 20 μm circular patterns at 80, 60, and 40 hPa. Images were taken by a confocal fluorescence microscope, and a 3D image was constructed. (C) Curvature radii and (D) curvatures obtained on SiO_2 circular patterns with diameters of 10, 20, and 30 μm at various pressures. Black lines are fittings by the transformed Young–Laplace equation.

pattern. The deviation of the image from partial sphere in Fig. 2B, larger at the position far from the glass surface, is the artifact due to the optical resolution of the confocal microscope in the *Z*-direction. The standard deviations in the estimation of the curvature radius and the curvature (reciprocal of curvature radius, Fig. 2D) were ~5%, that resulted in the volume variation of ~8%.

The relationship between the pressure and curvature radius can be fitted by the transformed Young–Laplace equation:[36]

$$1/R = \Delta P/2\gamma_{\text{water–oil}}$$

where R, ΔP, and $\gamma_{\text{water–oil}}$ are the curvature radius of the droplet, difference between the pressure inside and outside the droplet, and interfacial tension between water and oil, respectively. In this equation, maximum value of the ΔP for stable droplet formation is obtained when R reached the radius of the circular hydrophilic pattern, where the contact angle becomes $\pi/2$.[33,34] The curvature was found to be proportional to the applied pressure inside the micropipette (Fig. 2D). Using this relationship, we estimated $\gamma_{\text{water–oil}}$ to be 39.3 ± 0.8 mN/m. This value is slightly lower than those (52–54 mN/m) reported previously,[37,38] presumably due to the difference in the composition of the aqueous phase.

Slow leak of fluorescein from droplet

We investigated the possible leakage of fluorescein, which was used in the single-enzyme assay described in the next section. Although fluorescein has a negative charge at neutral pH and is highly soluble to water, its backbone structure consists of aromatic groups that can be soluble in less polar solvents. Fluorescein solution (1 μM) was injected into six droplets surrounding one droplet without fluorescein (Fig. 3A); the fluorescence intensity of each droplet was monitored for several tens of minutes. While the fluorescence intensities of the outer droplets decreased with time, that of the inner droplet slightly increased (Fig. 3B). Fig. 3C shows the time course of the fluorescence intensity. The decrease in fluorescence intensity of the outer droplets could be fitted by a single exponential decay curve. Under this condition, the time constant for the decrease in fluorescence intensity was 51 min. This result indicates that the leak of fluorescein from the droplet is relatively slow, since 51

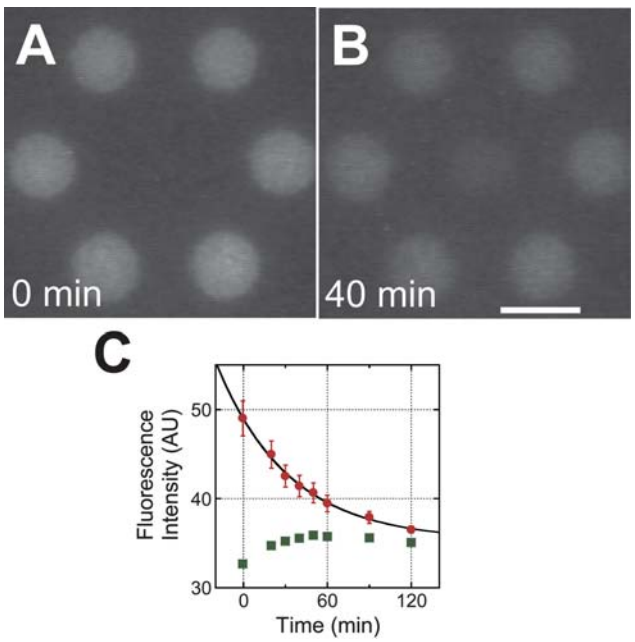

Fig. 3 Slow leak of fluorescein from droplet. (A and B) Fluorescence images of droplets which is 8.5 μm in diameter and has 6.5 μm intervals. Fluorescein solution (1 μM) was injected to the outer six droplets at 180 hPa. Images were taken at a rate of 30 fps and averaged over 5 frames. Scale bar: 10 μm. Images were taken just after preparation and after 40 min, respectively. (C) Time course of fluorescence intensity. Red circles and green squares indicate the fluorescence intensities of the outer six droplets and the droplet in the center, respectively. To suppress photobleaching, the excitation light was irradiated only at the time shown for ~1 s. The black line shows fitting by a single exponential decay function.

min is the lower limit when including the effect of photobleaching, and individual single-molecule measurements at least for several minutes can be done without considering concentration change.

Single-molecule enzymatic assay of β-galactosidase enclosed in a droplet

As a potential application of our accessible droplet array, the catalytic activity of β-galactosidase (β-gal) was measured at the single-molecule level (Fig. 4). β-gal hydrolyzes the fluorogenic substrate fluorescein-di-β-galactopyranoside (FDG) into fluorescein, and the reaction can be monitored by the increase in fluorescence. By mixing FDG solution with low concentration of β-gal and using it as the aqueous phase of the droplet array formation procedure (Fig. 1), we were able to enclose and detect single β-gal molecules in the droplet array very easily as previously reported using PDMS chamber (data not shown).[21] However, quantitative single-molecule measurement of catalytic activity was difficult since precise control of the droplet volume was difficult with this procedure. Therefore, we applied a micropipette to control the droplet volume.

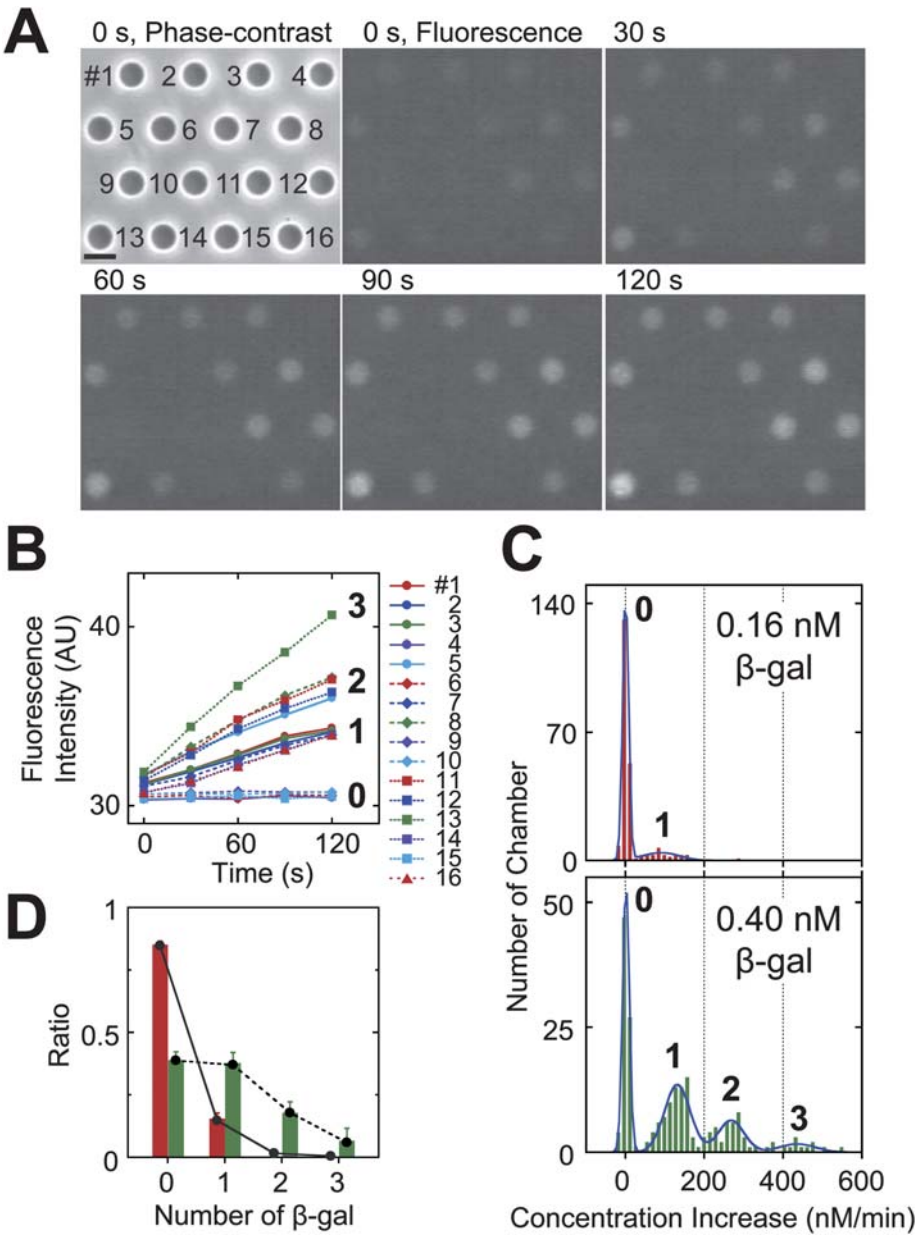

Fig. 4 Single-enzyme assay of β-gal. (A) Phase-contrast and fluorescence images of the droplet array with a 4.8 μm diameter and intervals of 5.2 μm. β-gal (0.40 nM in micropipette) was injected into each droplet at 290 hPa for ~1 s. Reaction was then started by the injection of 1 mM FDG at 300 hPa for ~1 s. Images were recorded at a rate of 30 fps and averaged over 11 frames. To suppress photobleaching, the excitation light was irradiated only at the time shown for ~1 s. Scale bar: 5 μm. (B) Time course for fluorescence intensity of the droplet. The numbers correspond to those shown in (A). (C) Distributions for the increasing rate of fluorescein concentration at 0.16 nM (top) and 0.40 nM (bottom) β-gal. Blue lines show the fitting by two (top) or four (bottom) Gaussian functions. (D) Ratio of droplets containing 0, 1, 2, or 3 β-gals at different concentrations of β-gals (red bars, 0.16 nM; green bars, 0.40 nM). The circles and lines indicate the fitting assuming the Poisson distributions.

We used a surface on which hydrophilic circular patterns with diameters of 4.8 μm were arrayed. We first prepared a droplet array containing the buffer solution. Then, 0.16 or 0.40 nM β-gal solution was injected at 290 hPa to yield a droplet with a volume of 14.8 fL, which was estimated from the results shown in Fig. 2. The injection into each droplet was finished in ~1 s. The reaction in each droplet was then started by the subsequent injection of the 1 mM FDG solution at 300 hPa. Under this condition, the final volume of the droplet was estimated to be 16.3 fL (Fig. 2). The final concentration of FDG in the droplet (>92 μM) was much higher than the Michaelis constant (18 μM) for the FDG hydrolysis by the β-gal,[39] and the β-gal exhibited a hydrolysis rate comparable to the maximum velocity.

Fig. 4A shows a time-series for the fluorogenic assay of β-gal, which was initiated by injection of 0.40 nM β-gal and 1 mM FDG. The fluorescence intensity of the individual droplets increased with time. Under this enzyme concentration, each droplet showed inhomogeneous fluorescent intensity, indicating the stochastic injection of β-gal molecules. The velocity of the fluorescence increase showed four discrete values, each corresponding to catalysis by 0, 1, 2, or 3 molecules of β-gal in the droplet, as confirmed below (Fig. 4B). The distributions of activity in each droplet are shown in Fig. 4C. The distribution showed two and four distinct peaks at 0.16 and 0.40 nM β-gal, respectively. These distributions could be fitted by the sum of two or four Gaussian functions. The intervals between the peaks of the Gaussian functions were essentially the same, indicating that 0 or 1 molecules of β-gal were enclosed in a droplet at 0.16 nM and that 0, 1, 2, or 3 molecules were enclosed at 0.40 nM. Using the interval between the peaks, we determined the turnover rate of a single β-gal enclosed in the droplet to be 14.7 ± 7.5 and 23.8 ± 13.2 s^{-1} for 0.16 and 0.40 nM β-gal, respectively. The error was chiefly due to the width of the Gaussian functions. Although the assay at 0.16 nM β-gal produced lower activity for unknown reasons, these results generally showed good agreement with previously reported turnover rates (17–20 s^{-1}).[21,39]

Next, we calculated the ratio for zero, one, two, and three β-gal molecules being contained in each droplet by comparing the areas of the Gaussian functions (Fig. 4D). The ratio obeyed the Poisson distribution, and the average number of β-gal molecules in the droplet was calculated to be 0.17 and 0.96 for 0.16 and 0.40 nM β-gal in the micropipette, respectively. These values were lower than the expected numbers of 1.4 and 3.6 for 0.16 nM and 0.40 nM β-gal, respectively. A possible explanation for this discrepancy is that β-gal molecules enclosed in a droplet may escape into the micropipette when FDG is injected. However, since the injection time was short (~1 s), this would be a minor reason (for equilibration between the droplet and micropipette, see the next section). Another possibility is that a significant fraction of β-gal in the micropipette is deactivated before injection due to non-specific binding to the inside glass surface of the micropipette. Since we did not coat the inside surface of the micropipette with a non-specific binding blocker like bovine serum albumin, this reason seems plausible. In contrast, once enclosed in the droplet, β-gal molecules were not deactivated at the interface between oil and water phase because fluorescence intensity from the droplet continued to increase for at least several minutes.

Determination of kinetic parameters for a single F_1-ATPase molecule

As a second application of the accessible droplet array to the single-molecule assay, we measured the rotation rates for a single F_1-ATPase (F_1),[30] a rotary motor protein, at various ATP concentrations ([ATP]). The rotation of F_1 can be directly visualized by attaching a large probe to the rotor γ subunit and by fixing the stator $\alpha_3\beta_3$ subunits on the glass surface. However, in a conventional flow cell with dimensions of millimeters and a volume of microliters, measurement of the rotation rate for a single F_1 at several [ATP] by buffer exchange is not so easy. The main difficulty is that a large volume of buffer should be flowing to completely exchange the flow cell content, and the flow during the buffer exchange can easily detach the probes from F_1 or F_1 from the glass surface. Therefore, in the conventional single-molecule assay of F_1, rotation rates are often measured at only one fixed [ATP] in one flow cell. A rotation assay in the droplet can reduce this problem because equilibration is easily achieved between the tiny volume of the droplet and the excess volume of micropipette and a strong flow does not occur during the [ATP] change.

When F_1, streptavidin-coated 220-nm polystyrene beads (a large probe), and 10 μM ATP were enclosed in droplets on hydrophilic circular patterns with diameters of 20 μm, rotating beads were observed. We did not control the chemistry to allow 1 : 1 reaction ratio between F_1 and bead, so there is a possibility that one bead binds to the multiple F_1 molecules. If the bead binds to multiple F_1 molecules on the glass surface, it will not rotate. Furthermore, there is a possibility that a single droplet contains multiple F_1 molecules that are bound or not bound with beads. So, to prevent ATP consumption by F_1 in droplet during observation, the ATP regenerating system was added.

After finding the rotation, [ATP] in the droplet was sequentially decreased by attaching new micropipettes (Femtochip, inside aperture 0.5 μm) filled with 1 and 0.5 μM ATP (Fig. 5A). The rotation rate of F_1 at each [ATP] was then calculated from the recorded images. Since the volume of the droplet was about 10^{-8} times smaller than that of the micropipette (on the order of several tens of microliters), [ATP] in the droplet became equal to that of the micropipette in a short time. The time required to achieve equilibration under the conditions used in rotation assay was estimated by the fluorescence imaging of the droplet containing fluorescein (Fig. 5B). During observations, the fluorescence intensity gradually decreased due to photobleaching (blue line). The time constant for photobleaching τ_{bleach} was determined to be 152.2 ± 10.8 s (mean ± SD, $n = 5$) by fitting of the exponential decay function: $A_1 \exp(-t/\tau_{bleach}) + B$. When the micropipette filled with buffer was attached to the droplet at 50 hPa during observations (arrow), the fluorescence intensity rapidly decreased due to diffusion of fluorescein into the micropipette (red line). The relaxation time τ_{relax} was determined to be 8.3 ± 0.6 s (mean ± SD, $n = 5$) by fitting the sum of the two exponential decay functions: $A_1 \exp(-t/\tau_{bleach}) + A_2 \exp(-t/\tau_{relax}) + C$, where τ_{bleach} was fixed at 152.2 s.

Fig. 5C shows a typical example of the time course for the rotation of a single F_1 molecule enclosed in a droplet. When [ATP] was decreased by attaching the micropipette for 30 s, the rotation rate decreased due to the lower ATP binding rate to F_1

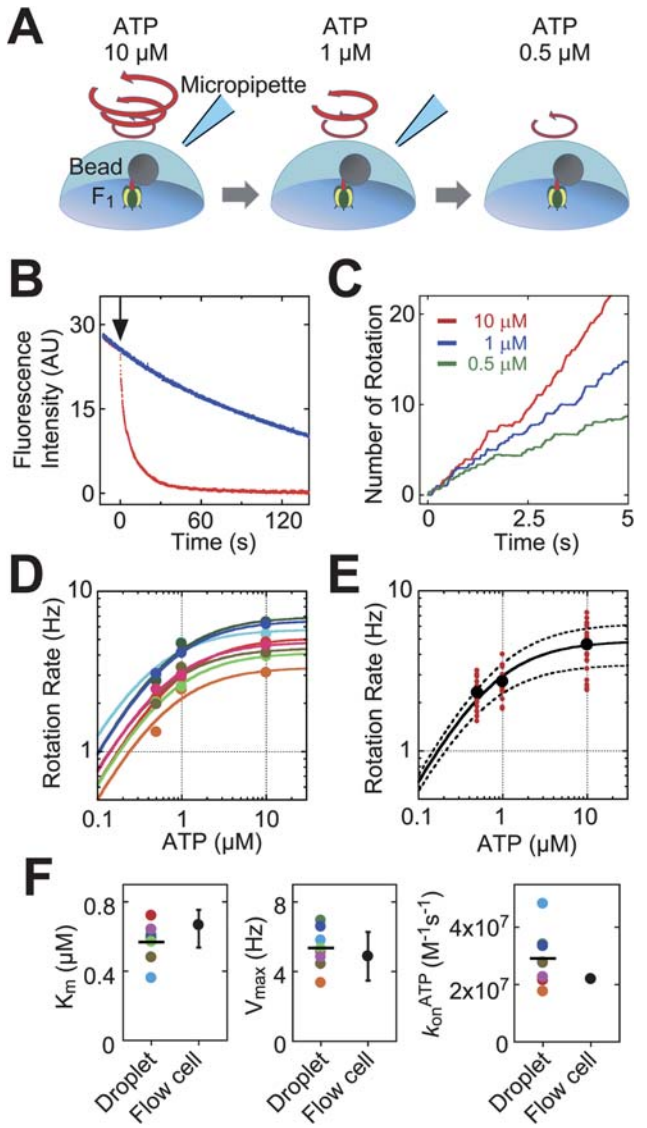

Fig. 5 Determination of kinetic parameters of single-molecule F_1-ATPase. (A) Schematic drawing of experimental set up (not to scale). The ATP concentration ([ATP]) was changed by attaching micropipettes filled with different [ATP] solutions. (B) Relaxation time after attachment of the micropipette to the droplet as measured by fluorescence imaging. During observation of the droplet containing 15 μM fluorescein (red line), a micropipette filled with buffer was attached at time zero at 50 hPa (arrow). The fluorescence intensity change due to photobleaching is also shown (blue line). (C) Example for time course of rotations of a single F_1 at different [ATP]. (D) Dependence of rotation rate on [ATP] in the droplet. Each color corresponds to the data from a single molecule. Lines are fitting curves by the Michaelis–Menten equation. (E) Dependence of rotation rate on [ATP] in the flow cell. Each red point corresponds to the data from different single molecules. Large circles are averaged values at each [ATP]. The solid line is the fitting curve by the Michaelis–Menten equation. The dashed lines indicate the width for the fitting considering the standard deviations for distribution. (F) Distributions of K_m, V_{max} and k_{on}^{ATP} as determined for single molecules of F_1. Colors correspond to the data shown in (D). Average values are indicated by horizontal lines. The values determined by flow cell experiments (E) are also shown (black circles).

at low [ATP] (Fig. 5D). The dependence of the rotation rate of F_1 on [ATP] obeys the Michaelis–Menten equation:[40]

$$v = V_{max} \{[ATP]/([ATP] + K_m)\}$$

where v, K_m, and V_{max} are the rotation rate, Michaelis constant, and maximum velocity, respectively. By fitting the results with the Michaelis–Menten equation we obtained the K_m and V_{max} of the individual F_1 molecules. The K_m and V_{max} values determined for individual F_1 molecules showed significant variation (Fig. 5F). The average values of K_m and V_{max} were 0.57 ± 0.11 μM and 5.3 ± 1.2 Hz (mean ± SD, $n = 8$), respectively. Although the variation was not small, the average values showed good agreement with those determined by the single-molecule assay using the conventional flow cell (Fig. 5E). In the flow cell experiment, K_m and V_{max} as determined by fitting the average rate at each [ATP] with the Michaelis–Menten equation were 0.66 μM and 4.9 Hz respectively, and their distributions were in the range of 0.52–0.78 μM and 3.5–6.3 Hz (Fig. 5E, F).

In the conventional flow cell assay, relatively large variations in the rotation rate of F_1 probed by an actin filament and a colloidal gold particle have been reported.[41,42] In our experiment using 220-nm latex beads as a probe, similar results were obtained; rotation rates at each [ATP] showed relatively large variations (Fig. 5E). A possible explanation for this variation is the difference in the drag coefficients of individual probes (bead aggregates) attached to the rotor of each F_1 molecule. However, in our assay in the droplet, we found that some F_1 molecules showed lower (higher) rotation rate than others at all [ATP] in addition to the variations between individual molecules (Fig. 5D). Furthermore, the values of k_{on}^{ATP} (= $3V_{max}/K_m$) for individual F_1 molecules, which correspond to the binding rate constant of ATP (F_1 hydrolyzes three ATP molecules per turn), showed significant variations (Fig. 5F). Although K_m and V_{max} for the rotation of F_1 is generally affected by the drag coefficient of the probe, k_{on}^{ATP} is independent of the load. These results suggest heterogeneity of the fundamental kinetic parameters, such as the ATP binding, hydrolysis and product release rates between individual F_1 molecules. Interesting phenomena for the conformational dynamics and catalysis of some enzymes, such as slow fluctuations, a memory effect, and dynamic disorder have been reported.[43–45] Investigation of the dynamic disorder for kinetics on F_1 would be an interesting topic for future study.

Conclusions

The femtoliter droplet array developed in this study has several advantages over previous femtoliter chambers, which have solid walls. Because each droplet is isolated by oil, the droplets can be accessed from outside. Precise control of the droplet volume, initiation and termination of the reaction, and exchange of the droplet content are possible. High-throughout quantitative assays of biological and chemical reactions with addressing of individual droplets can be realized under different conditions by combining this system with an automated micropipetting system. This femtoliter droplet array can be applied to the digital PCR and the digital ELISA, which detect very low amounts of DNA and diagnostic biomarkers down to the single-molecule level.[46,47]

Another important feature is the capability to recover the droplet content. This feature will be useful for further

applications of the accessible droplet array as a container for cell culture. In our preliminary experiments, single bacterial cells could be successfully cultured in the droplet and subsequently collected. By culturing the cells in the presence of a specific antibiotic, screening of the resistant bacteria and subsequent identification of the responsible gene for the resistance can be carried out.

Acknowledgements

This research was partly supported by the Program for Promotion of Fundamental Studies in Health Sciences of the National Institute of Biomedical Innovation, Japan (project ID: 07-3).

Notes and references

1 A. Manz, N. Graber and H. M. Widmer, *Sens. Actuators, B*, 1990, **1**, 244–248.
2 G. M. Whitesides, *Nature*, 2006, **442**, 368–373.
3 D. Janasek, J. Franzke and A. Manz, *Nature*, 2006, **442**, 374–380.
4 H. Craighead, *Nature*, 2006, **442**, 387–393.
5 G. M. Whitesides, E. Ostuni, S. Takayama, X. Jiang and D. E. Ingber, *Annu. Rev. Biomed. Eng.*, 2001, **3**, 335–373.
6 M. A. Unger, H. P. Chou, T. Thorsen, A. Scherer and S. R. Quake, *Science*, 2000, **288**, 113–116.
7 H. Wu, A. Wheeler and R. N. Zare, *Proc. Natl. Acad. Sci. U. S. A.*, 2004, **101**, 12809–12813.
8 L. Cai, N. Friedman and X. S. Xie, *Nature*, 2006, **440**, 358–362.
9 B. Huang, H. Wu, D. Bhaya, A. Grossman, S. Granier, B. K. Kobilka and R. N. Zare, *Science*, 2007, **315**, 81–84.
10 T. Thorsen, R. W. Roberts, F. H. Arnold and S. R. Quake, *Phys. Rev. Lett.*, 2001, **86**, 4163–4166.
11 S. L. Anna, N. Bontoux and H. A. Stone, *Appl. Phys. Lett.*, 2003, **82**, 364–366.
12 A. J. deMello, *Nature*, 2006, **442**, 394–402.
13 S. Y. Teh, R. Lin, L. H. Hung and A. P. Lee, *Lab Chip*, 2008, **8**, 198–220.
14 D. T. Chiu, R. M. Lorenz and G. D. Jeffries, *Anal. Chem.*, 2009, **81**, 5111–5118.
15 C. Holtze, A. C. Rowat, J. J. Agresti, J. B. Hutchison, F. E. Angile, C. H. Schmitz, S. Koster, H. Duan, K. J. Humphry, R. A. Scanga, J. S. Johnson, D. Pisignano and D. A. Weitz, *Lab Chip*, 2008, **8**, 1632–1639.
16 J. Clausell-Tormos, D. Lieber, J. C. Baret, A. El-Harrak, O. J. Miller, L. Frenz, J. Blouwolff, K. J. Humphry, S. Koster, H. Duan, C. Holtze, D. A. Weitz, A. D. Griffiths and C. A. Merten, *Chem. Biol.*, 2008, **15**, 427–437.
17 C. Priest, S. Herminghaus and R. Seemann, *Appl. Phys. Lett.*, 2006, **89**, 134101.
18 L. H. Hung, K. M. Choi, W. Y. Tseng, Y. C. Tan, K. J. Shea and A. P. Lee, *Lab Chip*, 2006, **6**, 174–178.
19 W. H. Tan and S. Takeuchi, *Lab Chip*, 2006, **6**, 757–763.
20 X. Niu, S. Gulati, J. B. Edel and A. J. deMello, *Lab Chip*, 2008, **8**, 1837–1841.
21 Y. Rondelez, G. Tresset, K. V. Tabata, H. Arata, H. Fujita, S. Takeuchi and H. Noji, *Nat. Biotechnol.*, 2005, **23**, 361–365.
22 L. Lam, S. Sakakihara, K. Ishizuka, S. Takeuchi and H. Noji, *Lab Chip*, 2007, **7**, 1738–1745.
23 L. Lam, R. Iino, K. V. Tabata and H. Noji, *Anal. Bioanal. Chem.*, 2008, **391**, 2423–2432.
24 R. Iino, L. Lam, K. V. Tabata, Y. Rondelez and H. Noji, *Jpn. J. Appl. Phys.*, 2009, **48**, 08JA04-01–08JA04-05.
25 D. M. Rissin and D. R. Walt, *Nano Lett.*, 2006, **6**, 520–523.
26 D. R. Walt, *Chem. Soc. Rev.*, 2010, **39**, 38–50.
27 S. Y. Jung, Y. Liu and C. P. Collier, *Langmuir*, 2008, **24**, 4439–4442.
28 Y. Hirono-Hara, K. Ishizuka, K. Kinosita Jr., M. Yoshida and H. Noji, *Proc. Natl. Acad. Sci. U. S. A.*, 2005, **102**, 4288–4293.
29 H. Noji, R. Yasuda, M. Yoshida and K. Kinosita Jr, *Nature*, 1997, **386**, 299–302.
30 Y. Rondelez, G. Tresset, T. Nakashima, Y. Kato-Yamada, H. Fujita, S. Takeuchi and H. Noji, *Nature*, 2005, **433**, 773–777.
31 Y. Iko, K. V. Tabata, S. Sakakihara, T. Nakashima and H. Noji, *FEBS Lett.*, 2009, **583**, 3187–3191.
32 L. Lam, S. Sakakihara, K. Ishizuka, S. Takeuchi, H. F. Arata, H. Fujita and H. Noji, *Biomed. Microdevices*, 2008, **10**, 539–546.
33 P. Lenz and R. Lipowsky, *Phys. Rev. Lett.*, 1998, **80**, 1920–1923.
34 H. Gau, S. Herminghaus, P. Lenz and R. Lipowsky, *Science*, 1999, **283**, 46–49.
35 S. Enoki, R. Watanabe, R. Iino and H. Noji, *J. Biol. Chem.*, 2009, **284**, 23169–23176.
36 A. W. Adamson and A. P. Gast, *Physical chemistry of surfaces*, Wiley, New York, 1997.
37 K. D. Dorfman, M. Chabert, J. H. Codarbox, G. Rousseau, P. de Cremoux and J. L. Viovy, *Anal. Chem.*, 2005, **77**, 3700–3704.
38 D. L. Chen, L. Li, S. Reyes, D. N. Adamson and R. F. Ismagilov, *Langmuir*, 2007, **23**, 2255–2260.
39 Z. J. Huang, *Biochemistry*, 1991, **30**, 8535–8540.
40 H. Gutfreund, *Kinetics for the life sciences: receptors, transmitters, and catalysts*, Cambridge University Press, Cambridge/New York, 1995.
41 R. Yasuda, H. Noji, K. Kinosita Jr. and M. Yoshida, *Cell*, 1998, **93**, 1117–1124.
42 R. Yasuda, H. Noji, M. Yoshida, K. Kinosita Jr. and H. Itoh, *Nature*, 2001, **410**, 898–904.
43 H. P. Lu, L. Xun and X. S. Xie, *Science*, 1998, **282**, 1877–1882.
44 B. P. English, W. Min, A. M. van Oijen, K. T. Lee, G. Luo, H. Sun, B. J. Cherayil, S. C. Kou and X. S. Xie, *Nat. Chem. Biol.*, 2006, **2**, 87–94.
45 D. M. Rissin, H. H. Gorris and D. R. Walt, *J. Am. Chem. Soc.*, 2008, **130**, 5349–5353.
46 E. A. Ottesen, J. W. Hong, S. R. Quake and J. R. Leadbetter, *Science*, 2006, **314**, 1464–1467.
47 D. M. Rissin, C. W. Kan, T. G. Campbell, S. C. Howes, D. R. Fournier, L. Song, T. Piech, P. P. Patel, L. Chang, A. J. Rivnak, E. P. Ferrell, J. D. Randall, G. K. Provuncher, D. R. Walt and D. C. Duffy, *Nat. Biotechnol.*, 2010, **28**, 595–599.

